AIAA JOURNAL
Vol. 31, No. 2, February 1993

Mixing Enhancement in Compressible Mixing Layers: An Experimental Study

E. M. Fernando*
QUEST Integrated, Inc., Kent, Washington 98032
and
S. Menon†
Georgia Institute of Technology, Atlanta, Georgia 30332

This paper presents results from an experimental study of mixing enhancement in compressible mixing layers. In this study, either helium or air was injected at Mach 1 from a tangential slot injector at a backward-facing step into a Mach 2.5 airstream. The tests consisted of studying the influence of various splitter plate geometries on the growth rate of the resulting mixing layer. The results indicate that the splitter plate geometry can significantly enhance the observed mixing-layer growth rates. The geometry that gave the greatest mixing enhancement resulted in a 380% increase in the mixing-layer growth rate and a twofold increase in the final mixing-layer thickness over the reference flat splitter plate case. Furthermore, the increase in mixing-layer thickness was seen almost exclusively on the lower Mach number side stream.

Nomenclature

M = Mach number
p = pressure
Re = Reynolds number
x = streamwise distance, origin at splitter plate trailing edge
y = vertical (floor-normal) distance, origin on floor
z = spanwise distance, origin on tunnel centerline
x,y,z = right-hand coordinate system
δ = boundary-layer thickness
δ^* = displacement thickness
θ = momentum thickness
χ = molar fraction

Subscripts
0 = stagnation conditions
1, 2 = primary and secondary stream, respectively
pt = pitot
r = reference condition, just upstream of splitter plate trailing edge
s = static

Introduction

SUCCESSFUL development of an airbreathing hypersonic aircraft requires the demonstration of a scramjet engine capable of sustaining thrust at very high Mach numbers. The diffusion combustion flame in the scramjet engine occurs only when the incoming supersonic airstream and the fuel (hydrogen) mix at the molecular level. Premixing the fuel and air is not feasible because of the high static temperature of the incoming airstream. Because of the high speed of the airstream within the combustor, the need for a combustor of reasonable length, and the fact that the growth rate of mixing layers decreases rapidly with increasing convective Mach number (Papamoschou,[1] Papamoschou and Roshko[2]), there has been great interest in the area of mixing augmentation for compressible mixing layers.

To date, several important techniques have been proposed for mixing augmentation. These include increasing the mixing-layer turbulence levels by an oscillating shock (Kumar et al.[3]) and techniques that enhance mixing by introducing streamwise vorticity into the mixing layer. Some experimental (Haas and Sturtevant,[4] Marble et al.[5]) and computational (Drummond et al.[6]) investigations have shown that baroclinic torques can be used toward this end. The technique relies on creating sharp pressure gradients that are not aligned with the mixing-layer density gradients. Alternatively, the normal injection techniques that have been studied by Carpenter[7] and Wang and George[8] also lead to high mixing rates due to the horseshoe vortex generated by the normal injection process (Settles and Dolling[9]). For the tests conducted here, the mixing layer was created by the tangential injection of the secondary stream. This injection method was preferred over normal injection as it inherently leads to lower stagnation pressure losses. To enhance mixing, several three-dimensional trailing-edge devices were built into the splitter plate that separates the two gas streams. It was theorized that these devices would lead to streamwise vorticity generation in the mixing layer, and hence to enhanced growth, due to the action of both baroclinic torques and the rotation of the spanwise vorticity vectors of the initial boundary layers. Hence, in the current tests, the efficiencies of several trailing-edge devices in augmenting mixing, and therefore the mixing-layer growth rate, were studied.

Experimental Facility

The experiments were carried out at the supersonic wind-tunnel facility at QUEST Integrated, Inc. This facility, which was completely designed and built during 1989, is a conventional supersonic blowdown wind tunnel that can operate at either Mach 2.5 or 3.5, with a nominal test section size of 8×8 cm. The current tests were carried out with the wind tunnel operating at Mach 2.5. The tunnel stagnation pressure range is between 0.41 and 1.0 MPa, which results in a freestream unit Reynolds number between 42×10^6 and 102×10^6 per meter At the nominal operating stagnation pressure of 0.66 MPa ($Re/\text{m} = 66.6 \times 10^6$), the facility can be operated continuously for approximately 1 min, with the capability of about 2.5 such operations per day. However, most data acquisition

Presented as Paper 91-1721 at the AIAA Fluid Dynamics, Plasma Dynamics, and Lasers Conference, Honolulu, HI, June 24-26, 1991; received Aug. 28, 1991; revision received June 5, 1992; accepted for publication June 6, 1992.

*Research Scientist; currently, Program Manager, Microsoft Corp., 1 Microsoft Way, Redmond, WA 98052. Member AIAA.
†Associate Professor, School of Aerospace Engineering. Member AIAA.

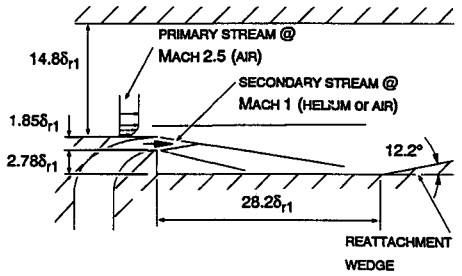

Fig. 1 Schematic showing experimental geometry.

runs only require the tunnel to operate continuously for less than 20 s. The wind-tunnel qualification tests have revealed that, under nominal operating conditions, the rms stagnation pressure fluctuation level is below 0.5% and the spanwise variation in the skin friction coefficient is less than $\pm 1.1\%$. Based on these and other measurements, the flow quality and spanwise uniformity in the wind tunnel have been judged to be good. As yet, no turbulence data have been acquired in this facility.

Test Conditions and Instrumentation

The current experimental geometry for the mixing augmentation studies is shown in Fig. 1. Briefly, the secondary stream (helium or air) is injected parallel to the primary stream (air), in a backward-facing step configuration. The primary stream is at Mach 2.5, whereas the secondary stream injection Mach number is nominally 1. For these test Mach numbers, when the injected gas is air, the mixing-layer convective Mach number is initially about 0.47, whereas for the helium injection case it is 0.29. The boundary layers on either side of the splitter plate form the initial mixing layer. The boundary-layer thickness on the primary stream side close to the trailing edge of the splitter plate, δ_{r1}, is 5.4 mm ($\delta^*_{r1} = 1.2$ mm, $\theta_{r1} = 0.276$ mm). On the secondary stream side of the splitter plate, these thicknesses are much smaller; δ_{r2} is estimated to be 0.2 mm, or $\delta_{r1}/27$. To determine the influence of the splitter plate on the mixing layer without the subsequent contamination due to streamline curvature introduced by reattachment on the tunnel floor, a ramp was installed downstream of the backward-facing step. This had the effect of making the mixing layer of interest more horizontal and thus reduced the influence of streamline curvature.

In designing the three-dimensional splitter plates, it was kept in mind that the appropriate scale for the trailing-edge devices is the boundary-layer thickness on the primary stream side. To minimize the shock wave strength in the freestream and the consequent stagnation pressure losses, the primary scale for the trailing-edge devices was $\approx 59\%$ of the primary stream side boundary-layer thickness, or 3.175 mm. Apart from the reference flat splitter plate, six other plates with three-dimensional trailing-edge devices were built. Three plates with varying aspect ratios (step width to step height) were built, as it was not clear a priori which geometry would lead to the greatest mixing enhancement. For the same reasons, two distinct tooth geometries (spanwise symmetric and asymmetric) were designed. Figure 2 shows details of the trailing-edge devices of these splitter plates.

To determine which splitter plate resulted in the greatest mixing enhancement, the ratio of the stagnation pressures of the injected stream to that of the primary stream and the reattachment wedge location were first adjusted so that the mixing layer evolved under conditions approaching those of a nominal zero-pressure gradient. Then the mixing-layer thickness was observed using the schlieren method. Once the plate that gave the greatest mixing enhancement was identified, a variety of surveys across the mixing layer were used, including pitot and static pressures, total temperature, and Rayleigh-scattering signal strength to determine the variation of the fluid mechanical parameters of interest.

The probes used for these tests were of standard design. They were introduced into the test section through the tunnel

	l_1/δ_{r1}	w_1/δ_{r1}	d_1/δ_{r1}	l_2/δ_{r1}	s_1/δ_{r1}
Asymmetric Splitter Plates					
63187	1.01	0.59	0.59	7.06	0
63188	1.01	0.59	0.59	7.06	0.59
63189	2.02	1.18	0.59	7.06	0
Symmetric Splitter Plates					
63190	1.01	1.18	0.59	7.06	0
63191	1.01	1.18	0.59	7.06	1.18
63192	2.02	2.36	0.59	7.06	0

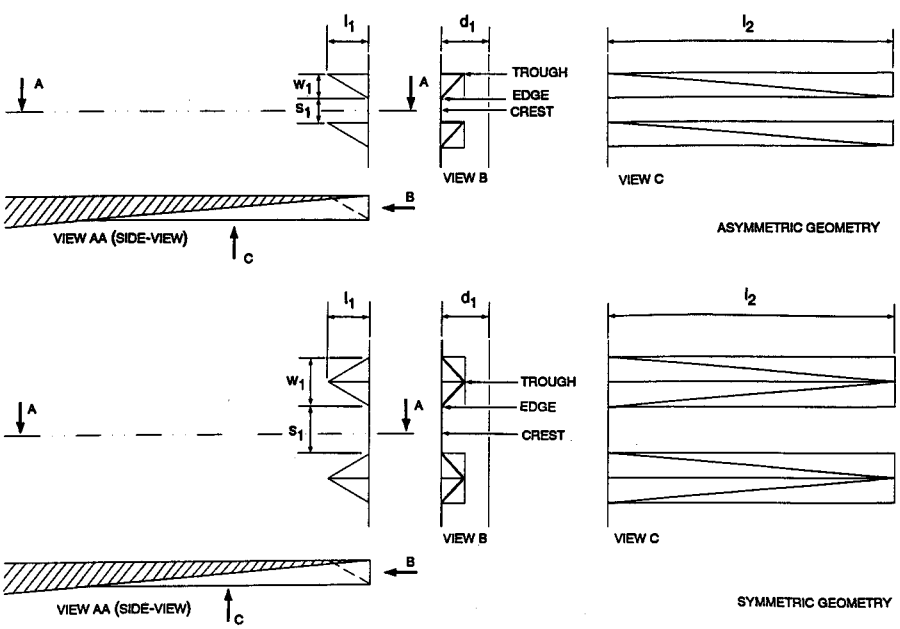

Fig. 2 Details of splitter plate three-dimensional trailing-edge devices.

floor and were traversed through the mixing layer. The pitot probe has a flattened tip (with an opening 0.08 mm high × 0.48 mm wide) to minimize streamline displacement effects in shear flows. The static pressure probe was a cone-cylinder probe with a 15-deg apex angle and two diametrically opposed static orifices (0.15-mm diam) located on a horizontal plane, approximately 10 cylinder diameters downstream from the tip. The total temperature was measured with an exposed-junction copper-constantan thermocouple.

For the air/air mixing layer, these three measurements alone were sufficient to obtain all of the parameters of interest. When the injection gas was changed to helium, however, another independent measurement was necessary. This measurement was the Rayleigh-scattering signal strength due to the gas molecules. The data reduction method then assumed the presence of two gasses with differing specific heat ratios; i.e., air was treated as one gas with a specific heat ratio of 1.4 and helium as another with a specific heat ratio of 1.67. This assumption is reasonable, since the relative difference in diffusion coefficients between oxygen into helium and nitrogen into helium is small. Furthermore, the current mixing-layer growth is believed not to be diffusion dominated but rather due to entrainment from vortex-induced mechanisms (Menon and Fernando[10]).

A schematic of the Rayleigh-scattering measurement setup is shown in Fig. 3. Briefly, linearly polarized light from a coherent laser at 514.5 nm is transmitted through the test section. A focusing lens insures a beam waist diameter of 70 μm at the measurement region of interest. A set of detection optics then images the Rayleigh-scattered light off this beam from the gas molecules onto six optical fibers, which in turn carry the light to six photomultipliers (Hamamatsu, R636). The amplified photomultiplier signals are filtered at 10 kHz and then digitized at 40 kHz. The sample volume for each photomultiplier is a region about 70 μm in diameter and about 1 mm in length. The use of six photomultipliers allows six equally spaced points with a total separation distance of about 6 mm to be imaged simultaneously, thus reducing the data acquisition time. Careful attention to the quality of the beam transmitting optics, along with painting the inside of the test section with a flat black paint, increased the Rayleigh-scattering signal-to-noise (background illumination) ratio to above 60.0 at the nominal test conditions. The ratio for the Rayleigh-

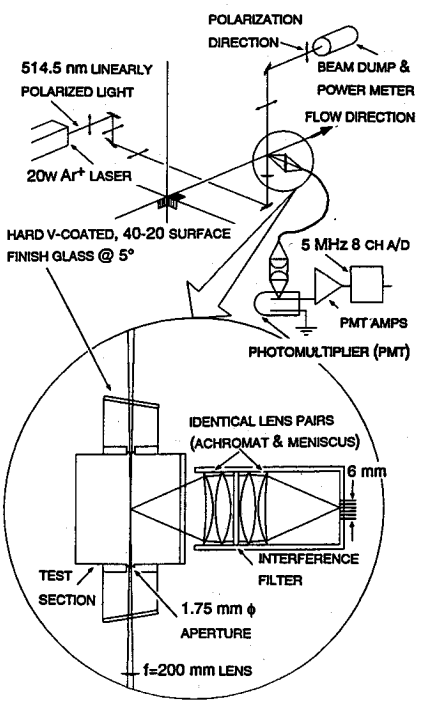

Fig. 3 Schematic of Rayleigh-scattering data acquisition setup.

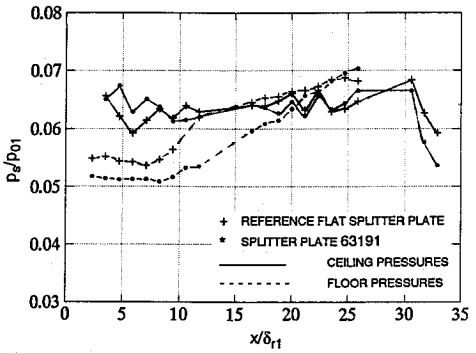

Fig. 4 Axial surface pressure distribution on tunnel centerline for two air/air mixing-layer cases.

scattering cross sections of air to helium is ≈ 66 (with air having the larger scattering cross section, see McCartney[11]). Hence, the pure helium signal and the background signal are of comparable magnitude. Although it is desirable to distinguish the helium signal above the background noise level, the vastly differing scattering cross sections of air and helium together with the existing signal-to-noise ratio enable the Raleigh-scattering results to be used to estimate the mixing-layer thickness.

A more important observation was that the Rayleigh-scattering measurements showed condensation effects in the Mach 2.5 airstream. This is believed to be caused by the homogeneous nucleation of the trace amounts of moisture present in the air supply (<80 ppm by weight). The effect of this phenomenon was to increase the mean Reyleigh-scattered signal level on the primary stream side. Since the presence of this condensation is dependent on the static temperature of the flow and its history, the use of the Rayleigh-scattered signal for obtaining the flow parameters of interest (such as Mach number, mass fraction, etc.) must be treated with caution (see also Shirinzadeh et al.[12] and Smith and Smits[13]). Additionally, small particles (<0.2 μm in diameter) were found in the secondary stream as well. These particles lead to spurious sharp spikes in time traces of the Rayleigh-scattered intensity. The Rayleigh-scattered signal was digitally processed to remove these spurious sharp spikes as well.

Air/Air Mixing-Layer Results

The initial mixing-layer tests were conducted using air as the injected gas, since the data reduction in this case required one less measurement (the Rayleigh-scattering intensity). These tests also provided a relatively inexpensive way to study the effects of the various splitter plates on the mixing-layer growth rate.

Figure 4 shows the axial surface pressure distribution for two test cases: the flat splitter plate and a three-dimensional splitter plate (63191 in Fig. 2). The stagnation temperatures for the two gas streams were close to the ambient temperature, whereas stagnation pressures were nominally 0.59 MPa for the primary airstream at Mach 2.5 and 0.061 MPa for the secondary airstream, which had a nominal injection Mach number of 1. It can be seen from Fig. 4 that the mixing layer develops under a mild adverse pressure gradient that is impossible to eliminate due to the backward-facing step configuration chosen for this study; however, the reattachment wedge greatly reduces the severity of the adverse pressure gradient. Schlieren images of the mixing layers obtained with these two plates confirmed that the mixing layer separates almost tangentially off the backward-facing step.

Vertical (i.e., floor-normal) pitot probe and static pressure probe traverses across the mixing layer have been used to measure the evolution of the shear layer with streamwise distance. In reducing the data for this case, it has been assumed that the total temperature is constant across the mixing layer. This is a reasonable assumption, as surveys have confirmed

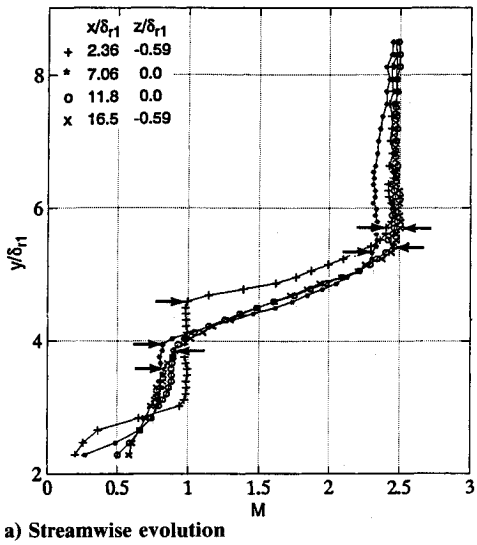

a) Streamwise evolution

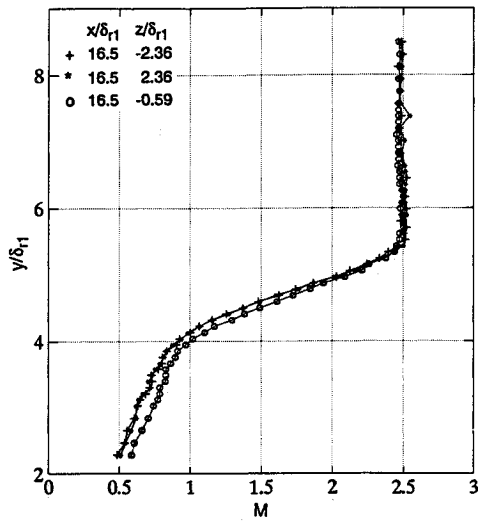

b) Spanwise uniformity at $x/\delta_{r1} = 16.5$

Fig. 5 Mach number profiles across air/air mixing layer created by reference flat splitter plate.

that the total temperature difference between the two gas streams is less than 3%.

Figure 5a shows Mach number profiles across the mixing layer for the reference flat plate case at several streamwise stations close to the tunnel centerline. These profiles show that initially the mixing layer is oriented slightly downward toward the tunnel floor before straightening out. They also clearly show the growth of the mixing layer with increasing streamwise distance. Even at the farthest downstream measurement station, the core of the secondary stream can be seen, which makes it possible to estimate the mixing-layer thickness. In this figure, the upper and lower edges of the mixing layer are noted by arrows; the streamwise evolution of the mixing-layer thickness is tabulated in Table 1. Figure 5b illustrates that, even at a far downstream measurement station, the spanwise variation in the mixing layer is quite small when the reference flat splitter plate is used.

For the case of the three-dimensional splitter plate, the mixing layer is inherently nonuniform in the spanwise direction. Figures 6a and 6b show profiles obtained at $x/\delta_0 = 2.36$ and 16.5 at three different spanwise locations. The spanwise nonuniformity, due to the trailing-edge devices, is clearly visible. These profiles have been marked as corresponding to the spanwise location of a crest, trough, or edge of the splitter plate trailing-edge devices (see Fig. 2). It is important to note that the spanwise variation in the mixing-layer thickness persists even at the farther downstream measurement station. Indeed, in this case it even appears that the spanwise variation increases with increasing downstream distance. It is expected that turbulent transport and diffusion will work to reduce this spanwise variation. However, organized structures such as streamwise vortices can lead to the observed persistence of the spanwise nonuniformity. It is also interesting to note that, unlike the behavior just described, another three-dimensional splitter plate (63190) did lead to spanwise nonuniformities that decreased with increasing streamwise distance (results not shown). Figure 7 shows the mixing-layer evolution in the streamwise direction at spanwise locations that correspond to the crests of the trailing-edge devices on splitter plate 63191.

The mixing-layer thickness data obtained from these figures are also summarized in Table 1. To obtain the mixing-layer

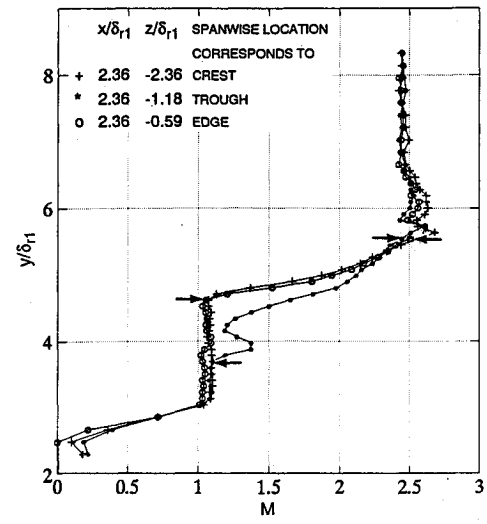

a) At $x/\delta_{r1} = 2.36$

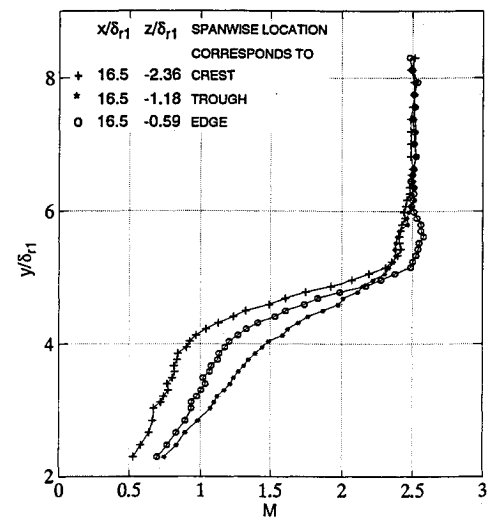

b) At $x/\delta_{r1} = 16.5$

Fig. 6 Mach number profiles across air/air mixing layer created by splitter plate 63191 showing spanwise variation.

Table 1 Mixing-layer thicknesses for air/air mixing-layer cases: C—spanwise measurement location corresponds to crest of trailing-edge device; similarly, E—edge and T—trough

	(Mixing-layer thickness)/δ_{r1}			
	Reference flat	Splitter plate 63191		
x/δ_{r1}	splitter plate	C	E	T
2.36	1.11	0.83	0.83	1.85
7.06	1.39	1.02	—	—
11.8	1.57	1.57	—	—
16.5	2.13	1.85	—	—

thickness from Figs. 6 and 7, it is first necessary to determine the upper and lower edges of the mixing layer. It is possible to determine the lower mixing-layer edge as a departure from the constant Mach number value in the freestream of the secondary stream. This determination is possible only where the freestream of the secondary stream is clearly visible. The determination of the upper edge of the mixing layer, at the axial station closest to the splitter plate trailing edge, when the

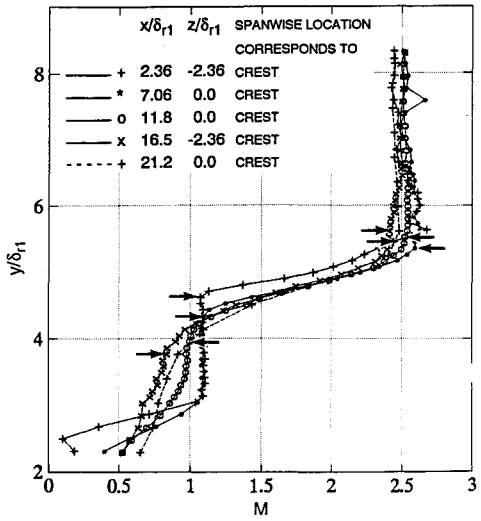

Fig. 7 Mach number profiles across air/air mixing layer created by splitter plate 63191 showing streamwise evolution.

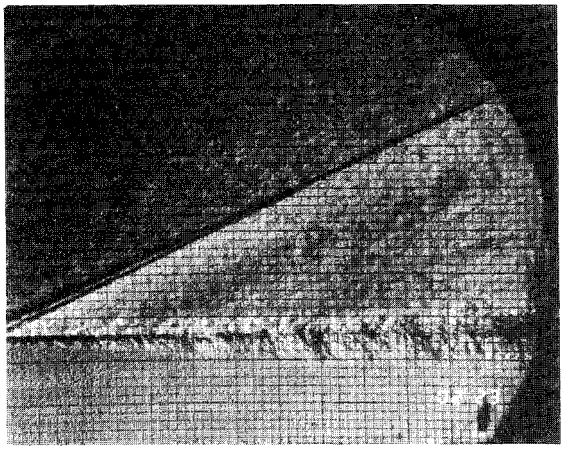

a) Mixing layer created by reference flat splitter plate

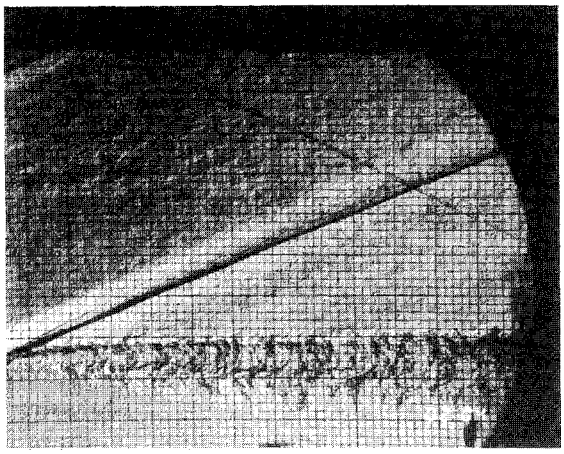

b) Mixing layer created by splitter plate 63192

Fig. 8 Side-view schlieren images for two helium/air mixing-layer cases. Graticule shows 2-mm squares; trailing edges of splitter plates are 1–3 mm to the left of images; flow is from left to right.

three-dimensional splitter plate is installed is somewhat subjective due to the propagation of the wave system, generated by the trailing-edge devices, across the mixing-layer upper edge. Here, the upper edge was determined to be at that height where the profile first reaches the value it attains in the primary stream freestream.

Note that for the three-dimensional plates the mixing-layer thickness is larger at spanwise locations that correspond to the troughs of the trailing-edge devices. Referring to the data in Table 1, and using the average mixing-layer thickness (at crest and trough) for splitter plate 63191, the initial mixing-layer thickness is 22% larger when splitter plate 63191 is installed, compared with when the reference flat splitter plate is installed. Furthermore, if it is assumed that the mixing-layer growth rate, Δ(mixing-layer thickness)/Δx, when the splitter plate 63191 is installed is the same at spanwise locations that correspond to trailing-edge device crests and troughs, then the mixing-layer growth rate for this case is 33% higher than for the reference case. These limited results illustrate that splitter plate geometry has a marked influence on augmenting mixing-layer growth rates.

Helium/Air Mixing-Layer Results

As described before, the first step in these tests was to match the stagnation pressure ratio between the two streams and the location of the reattachment wedge. For this series of tests, it was found unnecessary to change the reattachment wedge location from that of the previous tests. To closely match the ceiling and floor pressures and also to reduce the adverse pressure gradient on the tunnel floor, the primary stream stagnation pressure was set at 0.65 MPa, while the secondary stream stagnation pressure was set at 0.079 MPa.

Schlieren photographs were used to determine the mixing-layer thickness for all of the splitter plate shapes. The schlieren system employed a 1-μs duration flash source and was arranged in a classical Z-configuration. The data from these images are summarized in Table 2. Note that the greater mixing-layer thicknesses are observed with the plates that have trailing-edge devices of larger spanwise sizes. Figure 8 shows side views of the mixing layers for the reference flat splitter plate and the plate that resulted in the greatest mixing-layer growth rate (63192). Top views of the two cases reveal the existence of streamwise "structures" in the three-dimensional case (Fig. 9) with spanwise spacing that corresponds to the trailing-edge device spacing. The other three-dimensional splitter plates also initially led to streamwise structures that were not as persistent with increasing streamwise distance. These structures are not simply due to an undulation of the mixing layer; the thickness of the mixing layer does vary in the spanwise direction as was seen in the air/air results.

The tunnel surface pressures for these two cases are shown in Fig. 10. It can be seen that the floor and ceiling pressures for both splitter plates, within the region where profile measurements are taken, agree closely. The divergence of the ceiling pressures at the farther downstream locations is due to the impingement on the ceiling of the different wave systems generated by the two splitter plates. Figure 11 shows the streamwise evolution of the pitot pressure profiles for the flat splitter plate case. Because of the recirculation region and the low flow velocities, pitot pressure data closer than 10 mm to

Table 2 Visually observed mixing-layer thicknesses at $x/\delta_{r1} = 21.2$ for helium/air mixing-layer cases

Splitter plate	(Mixing-layer thickness)/δ_{r1}
Reference flat	2.04
63187	1.85
63188	2.04
63189	2.96
63190	2.04
63191	2.96
63192	3.70

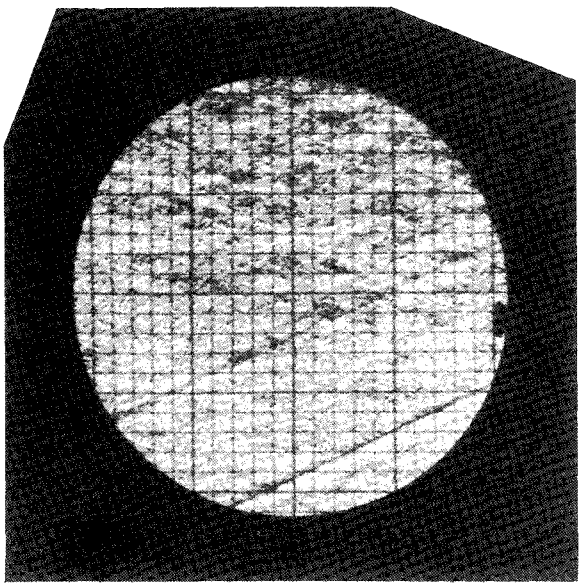

a) Mixing layer created by reference flat splitter plate

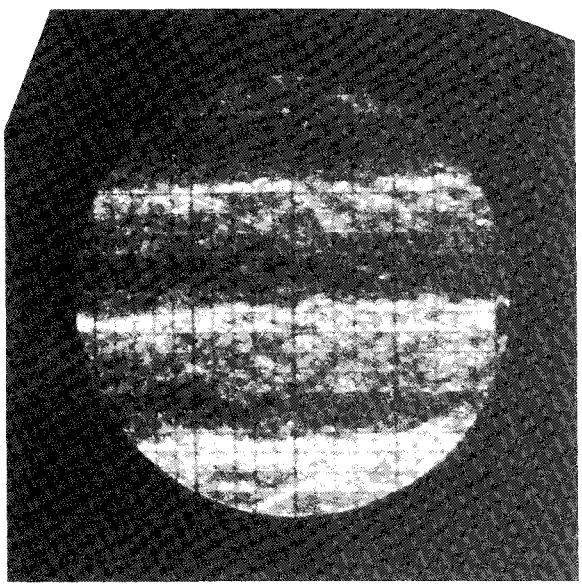

b) Mixing layer created by splitter plate 63192

Fig. 9 Top-view schlieren images for two helium/air mixing-layer cases. Graticule shows 2-mm squares; centers of images are at $x/\delta_{r1} = 7.06$, $z/\delta_{r1} = 0$; flow is from left to right.

the wall are unreliable and are not shown. Because of the low flow velocities close to the tunnel floor, continuous video schlieren monitoring was used during probe surveys to insure that the presence of the probe did not cause any unsteady flapping of the mixing layer or affect its orientation. Figure 11 does show the growth of the mixing layer with increasing downstream distance. The first two profiles also show the presence of a freestream core in the helium stream, which allows the thickness of the mixing layer to be determined at these stations.

Figure 12 shows corresponding streamwise pitot pressure profiles for the plate that resulted in the greatest mixing-layer growth rate. The evolution of the mixing-layer profiles obtained at spanwise positions corresponding to the troughs in a splitter plate trailing-edge device is seen to be quite different from those corresponding to the crests; the mixing layer is indeed thicker at locations corresponding to the troughs. Figure 13 shows a schematic of the spanwise appearance of the mixing layer by the farthest downstream measurement location for the case when splitter plate 63192 is installed. Whether the bulges in the mixing layer are actually counter-rotating vortices is not definitively known as yet.

Table 3 summarizes the mixing-layer thickness data for the two cases discussed so far. Also shown in Table 3 are mixing-layer thickness data obtained visually (schlieren, Fig. 8) and from the Rayleigh-scattering measurements. The mixing-layer thickness data were obtained from the Rayleigh-scattering measurements in the following manner. First, the Rayleigh-scattering intensity, together with the pitot and static pressures and the total temperature, is used to determine the molar fraction variation of air across the mixing layer. Figures 14a and 14b show two such profiles obtained with the two splitter

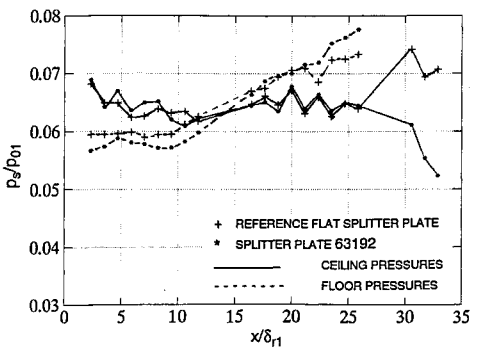

Fig. 10 Axial surface pressure distribution on tunnel centerline for two helium/air mixing-layer cases.

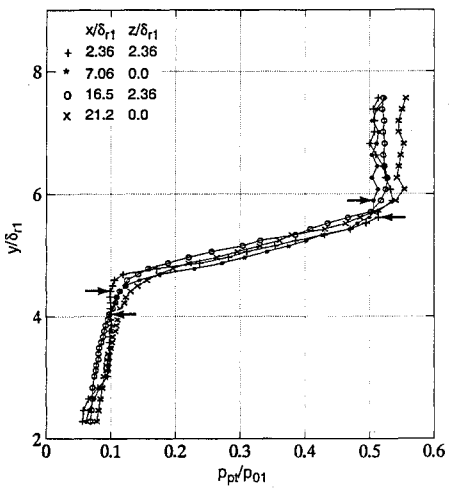

Fig. 11 Pitot pressure profiles across helium/air mixing layer created by reference flat splitter plate showing streamwise evolution.

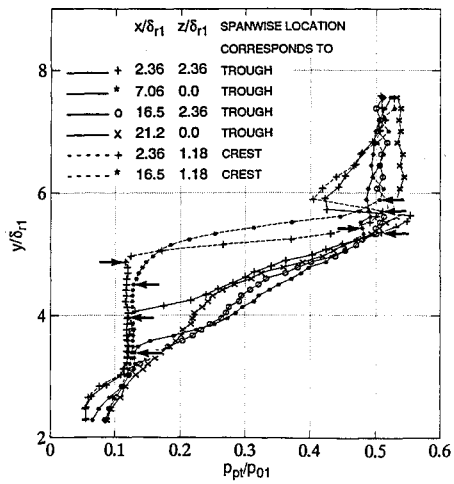

Fig. 12 Pitot pressure profiles across helium/air mixing layer created by splitter plate 63192.

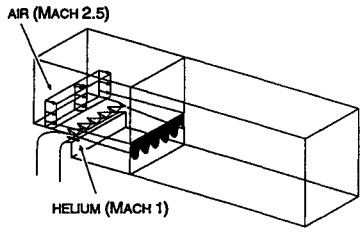

Fig. 13 Schematic showing spanwise variation of helium/air mixing-layer thickness created by splitter plate 63192.

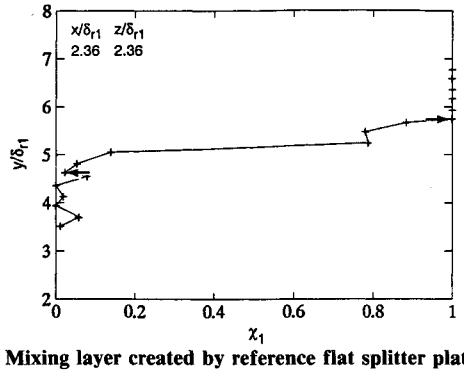

a) Mixing layer created by reference flat splitter plate

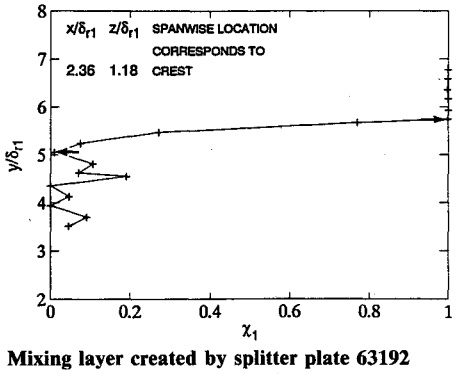

b) Mixing layer created by splitter plate 63192

Fig. 14 Profiles of the molar fraction of air across the helium/air mixing layer.

plate cases. From these profiles, the upper and lower edges of the helium/air mixing layer can be determined.

An important issue that needs to be addressed is what the mixing-layer thickness, as obtained from the pitot profile, schlieren image, and Rayleigh-scattering data, corresponds to; i.e., is it the vorticity thickness, velocity thickness, or some other measure? The mixing layer of interest is the one created between the air and helium streams; i.e., the mixing layer has two different gas species on either side of it. Furthermore, the static pressure variation across the mixing layer is generally negligible, and the Mach numbers, velocities, and stagnation pressures of the two gas streams are significantly different. For example, the helium freestream is nominally at Mach 1 with a velocity of 850 m/s, whereas the airstream is at Mach 2.5 with a velocity of 555 m/s and a stagnation pressure that is a factor of 8.2 higher than that in the helium stream. Hence, any mixing between the two gas streams will definitely lead to a change in the mass fraction of helium or air, a change in the velocity, and a change in the measured pitot pressure. For this reason it is felt that the mixing-layer thickness estimate with the pitot probe data should agree closely with an estimate of the mixing-layer thickness based on, say, the molar fraction of air or on an estimate based on the velocity thickness. Because of the nature of the complicated experimental geometry, which is tangential injection at a backward-facing step, there are a few exceptions to the previous statement. For example,

Table 3 Mixing-layer thicknesses for helium/air mixing-layer cases: C—spanwise measurement location corresponds to crest of trailing-edge device; similarly, E—edge, T—trough, P—mixing-layer thickness from pitot profile; similarly, R—from Rayleigh-scattered data, V—visual thickness from schlieren images

	(Mixing-layer thickness)/δ_{r1}		
	Reference flat	Splitter plate 63192	
x/δ_{r1}	splitter plate	C	T
2.36	1.11 P/1.11 R	0.83 P/0.69 R	1.39 P/2.41 R
7.06	1.85 P/1.11 R	—	2.04 P/2.49 R
16.5	1.38 R	1.39 P/2.49 R	2.83 R
21.1	1.80 R/2.04 V	—	3.33 R/3.7 V

the experimental geometry leads to the formation of two shear layers on either side of the helium injection slot. The upper layer is the one of interest to us. The lower one is initially a single-species (helium) mixing layer. Because of the merging of these two mixing layers at some downstream location, a mixing-layer thickness based on pitot probe data ceases to be relevant for the mixing layer of interest, whereas a thickness based on the molar fraction of air does not. Similarly, since the mixing layer of interest is created at the trailing edge of the splitter plate, where a thick air-side boundary layer exists, in the vicinity immediately downstream of the splitter plate trailing edge the mixing-layer thickness based on the pitot pressure profile and, say, the mass fraction of helium would not agree.

The mixing-layer thickness data in Table 3, obtained by these different methods, all show the same trend. However, there are some quantitative differences between the thickness data from the Rayleigh-scattering and pitot measurements, probably due to a combination of causes, including those discussed earlier and the sources of error in the Rayleigh-scattering measurements presented before. Some important results can be drawn from the data summarized in Table 3. A comparison of the average thickness of the mixing layers generated by the two splitter plates at the farthest streamwise station where spanwise measurements are possible ($x/\delta_{r1} = 16.5$) reveals that the mixing layer is 53% thicker when plate 63192 is installed. Note that this estimate uses the lesser of the two thickness values corresponding to spanwise location of the crest of plate 63192. A similar comparison at the first station ($x/\delta_{r1} = 2.36$) reveals that the thicknesses are the same for both cases. In terms of the mixing-layer growth rate, Δ(average mixing-layer thickness)/Δx between $x/\delta_{r1} = 2.36$ and 16.5, plate 63192 is 380% more effective than the reference flat plate. It is indeed this enhanced growth rate that results in the greater mixing-layer thickness at $x/\delta_{r1} = 16.5$ for plate 63192.

Concluding Comments

The primary objective of this work was to determine if splitter plate geometry can be used to enhance compressible mixing-layer growth rates. The results indicate that it is certainly possible. For the helium at Mach 1 and air at Mach 2.5 mixing layer, the most successful geometry increased the mixing-layer growth rate by 380% and the final average mixing-layer thickness by 53% over the reference flat plate geometry. Unfortunately, due to the limited test matrix, it was not possible to determine the best aspect ratio or spanwise size to achieve the greatest enhancement. However, the results do show that the spanwise size of the devices needs to be on the order of at least the initial boundary-layer thickness and not smaller. What was remarkable, however, was the observation that all of the enhanced growth of the mixing layer was on the lower Mach number stream side. It is likely that the subsonic flow on this stream side and the recirculation bubble provide a mechanism for the upstream propagation of flow information; this could be the reason for the observed behavior. The observation that the enhanced mixing does not occur on the higher Mach number air side has important implications from

the design point of a scramjet engine, due to the fact that the fuel/air mixing layer may not spread into the freestream if pressure-matched injection is used. In our laboratory tests, when the injection pressure was raised above the matched pressure condition, the mixing layer began to spread into the freestream and exhibited higher growth rates. However, the mixing layer exhibited unsteady oscillations and, hence, no reliable data acquisition was possible.

Acknowledgments

This work was carried out at QUEST Integrated, Inc., for the U.S. Air Force under Contracts F33615-88-C-2904 and F33615-89-C-2931 and was monitored by Tom Jackson at Wright-Patterson Air Force Base. This support is gratefully acknowledged. The authors are also indebted to Peter Seybert for his expert technical assistance in operating the wind tunnel and data acquisition system.

References

[1]Papamoschou, D., "Structure of the Compressible Turbulent Shear Layer," AIAA Paper 89-0126, Jan. 1989.

[2]Papamoschou, D., and Roshko, A., "The Compressible Turbulent Shear Layer: An Experimental Study," *Journal of Fluid Mechanics*, Vol. 197, Dec. 1988, pp. 453–477.

[3]Kumar, A., Bushnell, D. M., and Hussaini, M. Y., "A Mixing Augmentation Technique for Hypervelocity Scramjets," AIAA Paper 87-1882, June 1987.

[4]Haas, J.-F, and Sturtevant, B., "Interaction of Weak Shock Waves with Cylindrical and Spherical Gas Inhomogeneities," *Journal of Fluid Mechanics*, Vol. 181, Aug. 1987, pp. 41–76.

[5]Marble, F. E., Hendrick, G. J., and Zukoski, E. E., "Progress Toward Shock Enhancement of Supersonic Combustion Processes," AIAA Paper 87-1880, June 1987.

[6]Drummond, J. P., Carpenter, M. H., Riggins, D. W., and Adams, M. S., "Mixing Enhancement in a Supersonic Combustor," AIAA Paper 89-2794, July 1989.

[7]Carpenter, M. H., "Three-Dimensional Computations of Cross-Flow Injection and Combustion in a Supersonic Flow," AIAA Paper 89-1870, June 1989.

[8]Wang, J. H., and George, M. W., "Numerical Prediction of Hypersonic Combustor Flows," JANNAF Scramjet Combustor Modeling Workshop, Orlando, FL, July 19, 1990.

[9]Settles, G. S., and Dolling, D. S., "Swept Shock-Wave Boundary Layer Interactions," *Tactile Missile Aerodynamics*, edited by M. J. Hemsch and J. N. Nielsen, Vol. 104, Progress in Astronautics and Aeronautics, AIAA, New York, 1986, Chap. 8, pp. 297–379.

[10]Menon, S., and Fernando, E. M., "A Numerical Study of Mixing and Chemical Heat Release in Supersonic Mixing Layers," AIAA Paper 91-0152, Jan. 1991.

[11]McCartney, E. J., *Optics of the Atmosphere, Scattering by Particles and Molecules*, Wiley, New York, 1976.

[12]Shirinzadeh, B., Hillard, M. E., and Exton, R. J., "Condensation Effects on Rayleigh Scattering Measurements in a Supersonic Wind Tunnel," *AIAA Journal*, Vol. 29, No. 2, 1991, pp. 242–246.

[13]Smith, M. W., and Smits, A. J., private communication, Princeton Univ., Princeton, NJ, June 1990.